Light interference from single atoms and their mirror images

J. Eschner*†, **Ch. Raab***†, **F. Schmidt-Kaler**† & **R. Blatt**†

† *Institut für Experimentalphysik, Universität Innsbruck, Technikerstrasse 25, A-6020 Innsbruck, Austria*

* *These authors contributed equally to this work*

A single atom emitting single photons is a fundamental source of light. But the characteristics of this light depend strongly on the environment of the atom[1,2]. For example, if an atom is placed between two mirrors, both the total rate and the spectral composition of the spontaneous emission can be modified. Such effects have been observed using various systems: molecules deposited on mirrors[3], dye molecules in an optical cavity[4], an atom beam traversing a two-mirror optical resonator[5–8], single atoms traversing a microwave cavity[9–11] and a single trapped electron[12]. A related and equally fundamental phenomenon is the optical interaction between two atoms of the same kind when their separation is comparable to their emission wavelength. In this situation, light emitted by one atom may be reabsorbed by the other, leading to cooperative processes in the emission[13,14]. Here we observe these phenomena with high visibility by using one or two single atom(s), a collimating lens and a mirror, and by recording the individual photons scattered by the atom(s). Our experiments highlight the intimate connection between one-atom and two-atom effects, and allow their continuous observation using the same apparatus.

Single trapped ions have previously been used for studies of single-atom effects, examples being quantum jumps[15–17], antibunching[18], and deterministic entanglement[19]. Related experiments have been done with single molecules in solids (see ref. 20 for a review). In our experiment, single Ba$^+$ ions are trapped in an ion trap, laser-cooled, and well localized for hours. By retroreflecting the laser-induced fluorescence of a single ion with a lens and a distant mirror, we observe interference fringes with 72% visibility as the mirror distance varies. Simultaneous observation of the light transmitted through the mirror shows that the population of the upper level changes in anticorrelation with the interference fringes, which indicates genuine inhibition and enhancement of the atom's spontaneous emission. When two ions are trapped, they interfere with each other's mirror images, which indicates superradiance and subradiance mediated by the distant mirror. In this case the fringe visibility is 5%. The observed interference contrast, taking into account atomic motion and internal atomic dynamics, is in agreement with the theoretical prediction. The experiment also allows us to study the electromagnetic mode structure around a trapped ion and to determine its position with respect to the mirror with nanometre-resolution.

The experiment is described in Fig. 1. A direct and a retroreflected part of the resonance fluorescence of a single Ba$^+$ ion are recorded together on a photomultiplier while the distance between mirror and ion is varied. A scan of fluorescence versus mirror shift is shown in Fig. 2. Interference fringes appear which repeat when the mirror is shifted by half the 493-nm wavelength. The interference contrast (or visibility V) in this example is 72%. The observation shows clearly that light from the ion and from its mirror image, that is, light scattered by the same atom into opposite directions, is coherent and can therefore interfere.

As we will show below, there is the much deeper implication of a back-action on the atom, but first we study the interference signal by writing down an expression for the observed signal intensity, I, assuming an atom at rest and perfect wavefront matching between the two interfering field components

$$I = \langle |E(t-\tau) + E(t)|^2 \rangle = 2\langle |E(t)|^2 \rangle (1 + \mathrm{Re}[g^{(1)}(\tau)]) \quad (1)$$

Here $\langle \rangle$ denotes time averaging, $E(t)$ is the field component emitted directly into the detector and $\tau = 2(l + d)/c$ ($\approx$1.7 ns in Fig. 2) is the delay of the other component which reaches the detector after reflection by the mirror. In the second line of equation (1) we have used the definition of the first-order field correlation function

$$g^{(1)}(\tau) = \frac{\langle E^*(t-\tau)E(t) \rangle}{\langle |E(t)|^2 \rangle} \quad (2)$$

Obviously the last term in equation (1) contains the interference, and its amplitude when d is varied is the visibility,

$$V_{\mathrm{rest}} = |g^{(1)}(\tau)| \quad (3)$$

where the subscript rest indicates that atomic motion has not yet been taken into account.

The emitted field $E(t)$ can be expressed through the atomic polarization which itself is proportional to the atomic operator σ^- (ref. 21):

$$E(t) \propto \sigma^-(t) \quad (4)$$

so we can calculate $g^{(1)}(\tau)$ from the optical Bloch equations (OBEs) that describe the atomic dynamics. For the parameters of Fig. 2 we find (neglecting the back action) $V_{\mathrm{rest}} = 0.98$.

An experimental signature that the interference contrast depends on the internal dynamics of the atom is its dependence on the power of the exciting laser. The visibility is expected to diminish with increasing laser intensity owing to the increasing ratio of inelastic to elastic scattering[21]. In fact, we have observed such a reduction: typically, from $V > 50\%$ it decreases continuously to less than 10% when we change the laser intensity at 493 nm from below saturation to 3-fold saturation. This effect, however, arises only in part from the internal dynamics. It is also caused by the thermal motion of the ion, because laser cooling becomes less efficient when the laser intensity increases. A separation of the two contributions is the scope of future work.

Atomic motion influences the interference in the following way: The ion oscillates along the three axes of the trap, leading to a phase modulation of $E(t)$. A simple calculation shows that a sinusoidal oscillation with amplitude **x** decreases the interference contrast by a factor $J_0(\eta)$, where J_0 is the 0th-order Bessel function, $\eta = \mathbf{x}\mathbf{k_f}$ is the modulation index, and $\mathbf{k_f}$ is the fluorescence wave vector. Owing to the ongoing laser cooling, the motional state of the ion is thermal, which corresponds to a gaussian distribution of oscillation amplitudes. This leads to the interference contrast being modified to

$$V_{\mathrm{th}} = V_{\mathrm{rest}} I_0(\eta_{\mathrm{th}}^2) \exp(-\eta_{\mathrm{th}}^2) \quad (5)$$

where I_0 is the 0th-order modified Bessel function and $\eta_{\mathrm{th}} = \sqrt{\langle \eta^2 \rangle}$ is the average (thermal) modulation index.

By inserting into equation (5) the minimum thermal energy of the ion, corresponding to optimum laser cooling parameters, the maximum contrast which could be achieved is 93% for the highest trap frequencies. The reduction to the observed value of $V_{\mathrm{exp}} = 72\%$ arises partly from non-optimal cooling conditions, from fluctuations in the ion–mirror distance caused by acoustic noise, and from imperfect phasefront matching of the two interfering fields. Two sources of phasefront mismatch can be distinguished: distortions on the way to the mirror and back (for example, in the vacuum window) decrease the overall achievable contrast, whereas diffraction at the aperture of lens L1 leads to different phasefront curvatures of the backreflected light and the light emitted directly towards the detector. The latter effect enters into the effective solid angle for which interference takes place,
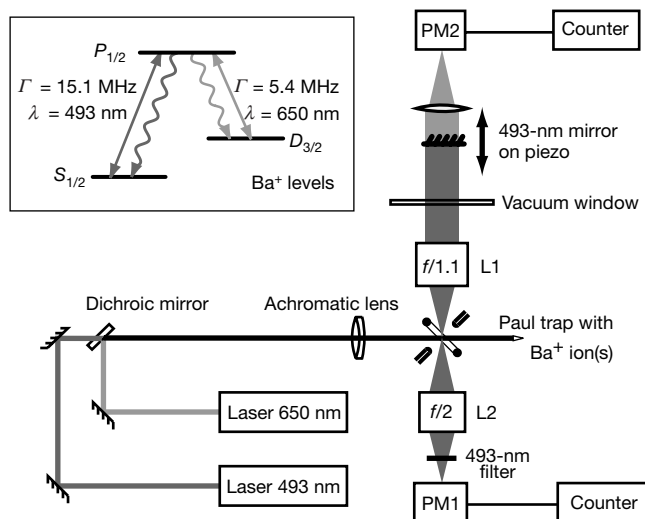
Figure 1 Experimental set-up (main figure) and relevant levels, transition wavelengths, and linewidths of Ba$^+$ (inset). A single Ba$^+$ ion is trapped in a Paul trap of 1.4 mm diameter. Its oscillation frequencies ω_z (ω_r) in the trap potential are between 1.2 and 2 (0.6 and 1) MHz. The ion is continuously laser-excited and laser-cooled on its $S_{1/2} \leftrightarrow P_{1/2}$ and $P_{1/2} \leftrightarrow D_{3/2}$ resonance lines. Both lasers have linewidths below 100 kHz; see refs 22 and 23 for details. The laser beams are combined on a dichroic mirror and focused into the trap. Both light fields are linearly polarized and their intensities are set roughly to saturation. The 650-nm laser is tuned close to resonance; the 493-nm laser is red-detuned by about the transition linewidth Γ for Doppler cooling. The precise parameters are determined by fitting a Bloch equation calculation to a scan of the fluorescence intensity versus laser detuning[24]. A high-quality lens L1 (f/1.1, wavefront aberration below λ/5) at right angles to the excitation beams and 12.5 mm away from the ion collimates the fluorescence light from a solid angle of ~4% into a parallel beam of 21.4 mm diameter. A mirror $l = 25$ cm away retroreflects the 493-nm part of this light while transmitting the 650-nm part. The mirror is angle-tuned for 180° back-reflection with a precision mirror mount and two piezo translators (PZTs). The retroreflected light is focused by L1 to the position of the ion and, together with the light emitted directly into that direction, it is collected with a second lens L2 and recorded with a photomultiplier (PM1). Coarse alignment, that is, superposition of the ion and its mirror image, is controlled visually through L2 while fine adjustment is done by optimizing the signal. The distance between mirror and ion is varied by an amount $d \simeq \pm 1\,\mu$m with another PZT. The 650-nm light transmitted through the mirror is recorded by a second photomultiplier PM2.

but it can be eliminated in the observed interference signal by making the aperture of L2 smaller than that of L1. We checked that an extra aperture stop in front of L2 did not increase the contrast.

In the simple model just presented we have not made use of the particular feature of this experiment that the two interfering light fields are superimposed at the position of the ion rather than on a beam splitter. The description given so far would apply to any beam-splitter model. In contrast, our retroreflecting lens–mirror set-up creates a back-action on the atom which is a fundamentally different effect. Intuitively, this back-action is explained by a modification of the electromagnetic vacuum at the position of the ion. The mirror creates nodes and antinodes in those modes which are collimated by the lens and then retroreflected, among them the modes which are analysed by the detector. The spontaneous emission rate into any of these modes is proportional to the mode intensity at the position of the ion, so we observe reduced or increased fluorescence depending on whether the ion is at a node or antinode; that is, depending on its distance from the mirror. Starting from that idea, the influence of the ion's internal dynamics and of its motion on the interference contrast can also be understood as spectral and spatial broadening,
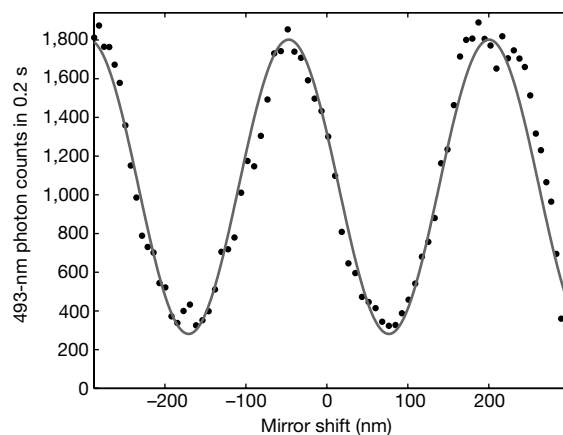
Figure 2 Self-interference in fluorescence of a single atom: photon count rate at PM1 versus mirror displacement (points). The fit (line) accounts for the nonlinear expansion of the PZT with applied voltage. We note that the probability that two photons are interfering is extremely small ($<10^{-5}$), which means that interference does indeed happen in each single emission event.

respectively; the broadening smears out the nodes and antinodes and therefore diminishes the interference contrast.

If some fraction of the total fluorescence is suppressed or enhanced, we also expect the total rate of fluorescence to vary at roughly the same percentage level. An observation of such a variation would verify that a back-action takes place. Therefore we recorded, simultaneously with the interference fringes, the fluorescence at 650 nm, which is transmitted through the mirror (see Fig. 1) and which is directly proportional to the population of the excited ($P_{1/2}$) level of the ion. The result is shown in Fig. 3. The 650-nm fluorescence exhibits a clear ~1% sinusoidal variation anticorrelated with the interference signal, indicating that an interference minimum (maximum) at 493 nm leads to higher (lower) population of the excited state. This shows that the mirror 25 cm away in fact acts on the internal atomic dynamics of the ion by modifying the population of the upper level.

The Methods section explains how this back-action is included into the description of the system by OBEs, the central point being that, in principle, it is indistinguishable whether a photon is emitted directly into the detector or via the mirror. A calculation with the OBEs accordingly modified and with the parameters of Fig. 3 predicts a variation of the total fluorescence by 0.9% if the effective fraction which can be brought to interference, including the various sources of visibility reduction, is set to 1.7%.

The fundamental aspects of the experiment, as described so far, also have fascinating practical implications: we can regard the set-up as a microscope to determine the position of the ion relative to the mirror. The precision of such a measurement is only limited by the noise in the photon-counting signal. It is estimated as follows. With an average count rate (per unit time) i_s and in a measurement interval of duration τ_{int}, we count $I_s = i_s\tau_{int}$ photons with a poissonian counting error of $\Delta I_s = \sqrt{I_s}$. The maximum slope of the interference signal versus mirror shift is $S = 2\pi A/(\lambda/2)$, where $A = V_{exp}I_s$ is the interference amplitude in the signal. Thus the error on I_s translates into an error of the position measurement:

$$\Delta x = \frac{\Delta I_s}{S} = \frac{\lambda/2}{2\pi V_{exp}\sqrt{i_s\tau_{int}}} \quad (6)$$

which amounts to 1.7 nm in the example of Fig. 2. This means that within a typical measurement time of 0.1 to 1 s the centre position of the ion can be determined more precisely than the extension of its
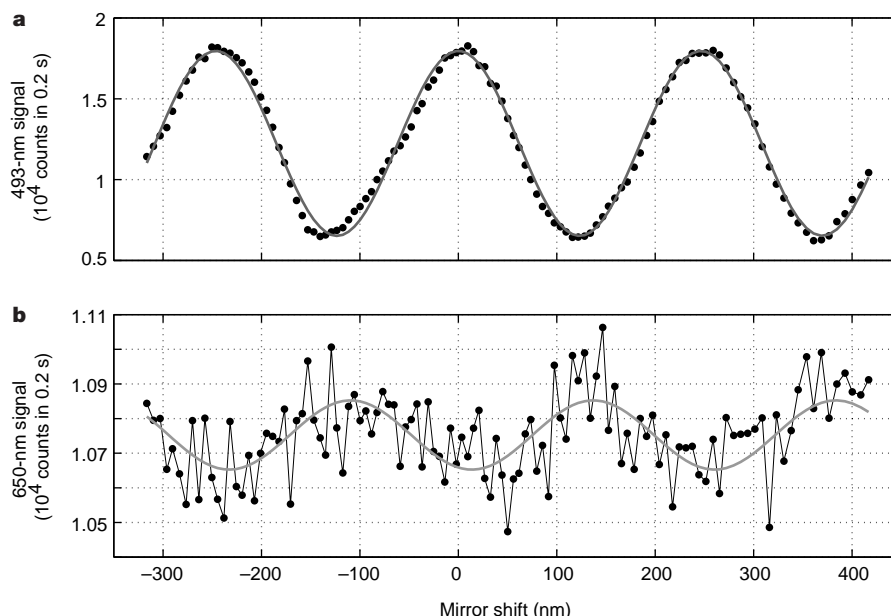
Figure 3 Interference fringes at 493 nm (**a**) and simultaneously recorded fluorescence at 650 nm transmitted through the mirror (**b**). Points are experimental data; bold lines are fits showing sinusoidal oscillations at the same frequency. The visibility of the modulation is 47% (**a**) and 0.9% (**b**). The visibility at 493 nm (**a**) is reduced compared to the measurement in Fig. 2 because the higher laser intensity that was used here did not permit optimum cooling. Within the experimental error (dominated by the counting noise in the 650-nm signal) the relative phase of the fits is in agreement with anticorrelation, as predicted by the model.
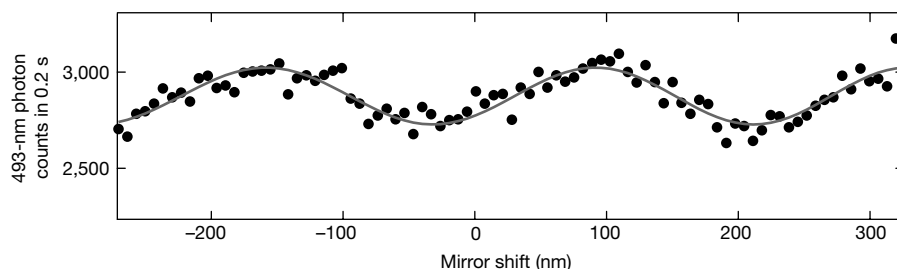
Figure 4 Interference fringes as in Fig. 2 but now with two ions, each interfering with the mirror image of the other. The visibility is about 5%; the main reason for its reduction, compared to the one-ion experiment, is the strongly driven (micro-) motion of the ions in the Paul trap when their mutual repulsion displaces them from the trap centre.

ground state wave packet in the trap (~7 nm). The precision can be increased further by increasing the integration time, which opens up exciting possibilities of measuring and even manipulating the position and motion of the ion on a scale below its position uncertainty. In the same sense, our interference signal reveals spatial variations in the electromagnetic mode structure around the ion on a sub-optical scale; here the resolution is set by the thermal wave packet (~35 nm).

We now show that the single-atom phenomena described so far are intimately connected to another fundamental process, namely superradiance and subradiance, which is the cooperative spontaneous emission (or its inhibition) of at least two atoms[13]. With the same set-up as before but with two laser-cooled ions in the trap, we adjust the mirror such that the mirror image of each ion is superimposed with the real image of the other ion. When we scan the mirror we find a result as displayed in Fig. 4. Again, interference fringes appear with the same period as before and with about 5% contrast. However, their interpretation must certainly be different because it is not light from the same atom that interferes, nor is there a back-action of an atom on itself. Instead, the two indistinguishable processes which create the interference are emission by one ion towards the detector and emission by the other towards the mirror, and the two atoms interact with each other.

Inspection of the model for this two-atom case (see the Methods section) reveals the interaction to be reabsorption by one atom of photons emitted by the other. This shows that the observed interference is in fact a signature of subradiance and superradiance. In an earlier experiment[14] the corresponding lifetime modification was studied with two ions spaced by about 1.5 μm in a strongly confining trap. In our case, direct interaction between the atoms over their separation of 5 μm would not be observable. Instead, the interaction mediated by the mirror over a distance of 50 cm produces a clear and unambiguous effect. □

Methods

The optical Bloch equations (OBEs) derive from a master equation for the atomic density operator ρ, which incorporates the quantum dynamics of the laser-excited atom and the dissipative processes such as spontaneous emission. To include the back-action created by the mirror into the description of the system we have to take into account that the two directions in which a photon can be emitted before it reaches the detector are indistinguishable. This enters into the OBEs in the following way: the term representing dissipation in the master equation is

$$(\dot{\rho})_{\mathrm{diss}} = -\frac{1}{2}\sum_n C_n^\dagger C_n \rho + \rho C_n^\dagger C_n - 2C_n \rho C_n^\dagger \qquad (7)$$

where the operators C_n (and their hermitian adjoints $C_n^\dagger$) stand for the different dissipative mechanisns. In particular, spontaneous decay is described by $C = \sqrt{\Gamma}\sigma^-$, the operator σ^-

denoting transitions from the upper to the lower atomic state. This total spontaneous emission can be decomposed, without changing equation (7), into parts $C_1 = C_2 = \sqrt{\Phi\Gamma}\sigma^-$ and $C_3 = \sqrt{(1 - 2\Phi)\Gamma}\sigma^-$, which stand for spontaneous emission in the direction of the detector, in the opposite direction (towards the mirror), and in the remaining solid angle, respectively. The action of the mirror is now described by replacing C_1 and C_2 in equation (7) by the coherent sum

$$C_{12} = C_1 + e^{-i\omega_1\tau}C_2 = \sqrt{\Phi\Gamma}(1 + e^{-i\omega_1\tau})\sigma^- \qquad (8)$$

with laser frequency ω_1, and Φ denoting the effective fraction of the total fluorescence which can be brought to interference, including the contrast reduction by atomic motion, by $g^{(1)}$, and by wavefront distortions. Equation (8) models precisely the situation where the decay that the detector observes is the superposition of the two possible directions, one being delayed by τ. An OBE calculation with this modified dissipation predicts a variation of the total fluorescence with the ion–mirror distance at a level determined by Φ. This is inhibited and enhanced spontaneous emission; it can also be regarded as resulting from reabsorption or stimulated emission induced by the back-reflected photons.

In the two-ion case, the two indistinguishable processes which interfere are emission by one ion towards the detector and emission by the other ion towards the mirror. Using the same tools as above, we model the situation by adding coherently the two decay processes C_{a1} and C_{b2} (and vice versa) where now a and b label the ions and 1 and 2 label the directions of emission. The two new decay operators are given by

$$C_{ab} = C_{a1} + e^{-i\omega_1\tau}C_{b2}; \quad C_{ba} = C_{b1} + e^{-i\omega_1\tau}C_{a2}. \qquad (9)$$

When these are introduced into equation (7) (now ρ is the two-atom density matrix), then a term $(\sigma_a^+\sigma_b^- + \sigma_b^+\sigma_a^-)\cos(\omega_1\tau)\rho$ appears in the OBEs, which describes simultaneous emission by one ion and absorption by the other and which is modulated with the distance between the ions via the mirror. This shows that in fact reabsorption (and its inhibition) of the emitted photons goes along with the observed interference. A slightly different viewpoint is that, depending on the phase factor $e^{i\omega_1\tau}$, either the symmetric or the antisymmetric two-atom wave function is preferentially populated, which leads to enhanced or suppressed collective spontaneous emission, respectively. This is subradiance and superradiance as originally described by Dicke[13].

1. Purcell, E. M. Spontaneous emission probabilities at radio frequencies. *Phys. Rev.* **69,** 681 (1946).
2. Milonni, P. W. *The Quantum Vacuum* Ch. 6 (Academic, San Diego, 1994).
3. Drexhage, K. H. in *Progress in Optics* (ed. Wolf, E.) Vol. 12, 163–232 (North-Holland, Amsterdam, 1974).
4. DeMartini, F., Innocenti, G., Jacobovitz, G. R. & Mataloni, P. Anomalous spontaneous emission time in a microscopic optical cavity. *Phys. Rev. Lett.* **59,** 2955–2958 (1987).
5. Jhe, W. *et al.* Suppression of spontaneous decay at optical frequencies: Test of vacuum-field anisotropy in confined space. *Phys. Rev. Lett.* **58,** 666–669 (1987).
6. Heinzen, D. J., Childs, J. J., Thomas, J. F. & Feld, M. S. Enhanced and inhibited visible spontaneous emission by atoms in a confocal resonator. *Phys. Rev. Lett.* **58,** 1320–1323 (1987).
7. Hood, C. J., Lynn, T. W., Doherty, A. C., Parkins, A. S. & Kimble, H. J. The atom-cavity microscope: Single atoms bound in orbit by single photons. *Science* **287,** 1447–1453 (2000).
8. Pinkse, P. W. H., Fischer, T., Maunz, P. & Rempe, G. Trapping an atom with single photons. *Nature* **404,** 365–368 (2000).
9. Goy, P., Raimond, J. M., Gross, M. & Haroche, S. Observation of cavity-enhanced single-atom spontaneous emission. *Phys. Rev. Lett.* **50,** 1903–1906 (1983).
10. Hulet, R. G., Hilfer, E. S. & Kleppner, D. Inhibited spontaneous emission by a Rydberg atom. *Phys. Rev. Lett.* **55,** 2137–2140 (1985).
11. Rempe, G., Walther, H. & Klein, N. Observation of quantum collapse and revival in a one-atom maser. *Phys. Rev. Lett.* **58,** 353–356 (1987).
12. Gabrielse, G. & Dehmelt, H. G. Observation of inhibited spontaneous emission. *Phys. Rev. Lett.* **55,** 67–70 (1985).
13. Dicke, R. H. Coherence in spontaneous radiation processes. *Phys. Rev.* **93,** 99–110 (1954).
14. DeVoe, R. G. & Brewer, R. G. Observation of superradiant and subradiant spontaneous emission of two trapped ions. *Phys. Rev. Lett.* **76,** 2049–2052 (1996).
15. Nagourney, W., Sandberg, J. & Dehmelt, H. Shelved optical electron amplifier: Observation of quantum jumps. *Phys. Rev. Lett.* **56,** 2797–2799 (1986).
16. Sauter, Th., Neuhauser, W., Blatt, R. & Toschek, P. E. Observation of quantum jumps. *Phys. Rev. Lett.* **57,** 1696–1698 (1986).
17. Bergquist, J. C., Hulet, R. G., Itano, W. M. & Wineland, D. J. Observation of quantum jumps in a single atom. *Phys. Rev. Lett.* **57,** 1699–1702 (1986).
18. Diedrich, F. & Walther, H. Nonclassical radiation of a single stored ion. *Phys. Rev. Lett.* **58,** 203–206 (1987).
19. Sackett, C. A. *et al.* Experimental entanglement of four particles. *Nature* **404,** 256–259 (2000).
20. Moerner, W. E. in *Atomic Physics 14* (eds Wineland, D. J., Wieman, C. E. & Smith, S. J.) AIP Conf. Proc. Vol. 323, 467–486 (AIP Press, New York, 1995).
21. Loudon, R. *The Quantum Theory of Light* (Oxford Univ. Press, Oxford, 1983).
22. Raab, C. *et al.* Diode laser spectrometer at 493 nm for single trapped Ba^+ ions. *Appl. Phys. B* **67,** 683–688 (1998); *Appl. Phys. B* **69,** 253 (1999).
23. Raab, C. *et al.* Motional sidebands and direct measurement of the cooling rate in the resonance fluorescence of a single trapped ion. *Phys. Rev. Lett.* **85,** 538–541 (2000).
24. Schubert, M., Siemers, I., Blatt, R., Neuhauser, W. & Toschek, P. E. Transient internal dynamics of a multilevel ion. *Phys. Rev. A* **52,** 2994–3006 (1995).

Bose–Einstein condensation on a microelectronic chip

W. Hänsel, P. Hommelhoff, T. W. Hänsch & J. Reichel

Max-Planck-Institut für Quantenoptik und Sektion Physik der Ludwig-Maximilians-Universität, Schellingstr. 4, D-80799 München, Germany

Although Bose–Einstein condensates[1–3] of ultracold atoms have been experimentally realizable for several years, their formation and manipulation still impose considerable technical challenges. An all-optical technique[4] that enables faster production of Bose–Einstein condensates was recently reported. Here we demonstrate that the formation of a condensate can be greatly simplified using a microscopic magnetic trap on a chip[5]. We achieve Bose–Einstein condensation inside the single vapour cell of a magneto-optical trap in as little as 700 ms—more than a factor of ten faster than typical experiments, and a factor of three faster than the all-optical technique[4]. A coherent matter wave is emitted normal to the chip surface when the trapped atoms are released into free fall; alternatively, we couple the condensate into an 'atomic conveyor belt'[6], which is used to transport the condensed cloud non-destructively over a macroscopic distance parallel to the chip surface. The possibility of manipulating laser-like coherent matter waves with such an integrated atom-optical system holds promise for applications in interferometry, holography, microscopy, atom lithography and quantum information processing[7].

Some of the advantages of microscopic magnetic traps on a chip have been pointed out before. Modest electric currents can produce large magnetic field gradients and curvatures in close proximity to a planar arrangement of wires[8]. In an experiment which was realized simultaneously with the results reported here, microfabricated parallel conductors were used in a last stage of evaporative cooling to achieve Bose–Einstein condensation (BEC)[9]. Lithographic fabrication techniques now make it possible to integrate even complex systems of many microscopic traps, waveguides[10,11], and other atom-optical devices[12–14] on a single 'atom chip'.

The use of such microtraps for BEC appears, in hindsight, only natural, as quantum-mechanical phenomena tend to be more readily observable on a smaller scale. A tight trap permits fast adiabatic changes of the confining potential, and it becomes easy to magnetically compress a trapped atom cloud so that elastic collision times of the order of milliseconds are reached even with just a few million trapped atoms. The resulting fast thermalization makes it possible to drastically shorten the time for radio-frequency-assisted evaporative cooling[15]. It is also advantageous that a tight magnetic confinement positions the atom cloud near the centre of the magnetic trap, despite the pull of gravity, so that a rather uniform evaporation is achieved throughout the evaporation process. Collisions with background gas atoms become less important during such a fast cooling cycle, so that the previously very stringent requirements on the vacuum may be greatly relaxed.

Figure 1a shows the chip that is used in our BEC experiments. It features 50-μm-wide conductors, which reproducibly support continuous currents in excess of 3 A. The chip was fabricated